Taylor & Francis
Taylor & Francis Group

Vehicle System Dynamics
International Journal of Vehicle Mechanics and Mobility

ISSN: (Print) (Online) Journal homepage: https://www.tandfonline.com/loi/nvsd20

Prediction of coupling effect between pantograph and tunnel resulting from car body vibration using an aerodynamic and multi-body dynamic coupling approach

Zhanling Ji, Yi Guo, Dilong Guo, Guowei Yang & Jun Mao

To cite this article: Zhanling Ji, Yi Guo, Dilong Guo, Guowei Yang & Jun Mao (2023): Prediction of coupling effect between pantograph and tunnel resulting from car body vibration using an aerodynamic and multi-body dynamic coupling approach, Vehicle System Dynamics, DOI: 10.1080/00423114.2023.2189125

To link to this article: https://doi.org/10.1080/00423114.2023.2189125

VEHICLE SYSTEM DYNAMICS
https://doi.org/10.1080/00423114.2023.2189125

Prediction of coupling effect between pantograph and tunnel resulting from car body vibration using an aerodynamic and multi-body dynamic coupling approach

Zhanling Ji[a], Yi Guo[a], Dilong Guo[a], Guowei Yang[a] and Jun Mao [b]

[a]Institute of Mechanics, Chinese Academy of Sciences, Beijing, People's Republic of China; [b]School of civil engineering, Beijing Jiaotong University, Beijing, People's Republic of China

ABSTRACT

An aerodynamic and multi-body dynamic coupling method is proposed and verified to evaluate the coupling effect between a pantograph on a high-speed train and the tunnel resulting from the train's vibration. The unevenness of the catenary, posture changes of the car body, track irregularities, tunnel effect and the interactions between the air and rods are considered. The influence and the evolution of the car body's vibration on the service characteristics and responses of the pantograph are described and quantified from multiple perspectives, including the time-domain characteristics of the aerodynamic lift of the panhead, the contact force between the pantograph and catenary, the vertical displacement and vertical acceleration of the contact strip, the frequency-domain characteristics, and the phase diagram of the contact strip. New insights are obtained into the action mechanisms of the car body vibration on the coupling effect between the pantograph and tunnel.

ARTICLE HISTORY
Received 11 January 2022
Revised 16 May 2022
Accepted 3 August 2022

KEYWORDS
Coupling effect between pantograph and tunnel; high-speed trains; car body vibration; aerodynamic and multi-body dynamic coupling; pantograph

1. Introduction

A high-speed train obtains electrical energy from the catenary through the pantograph and transmits it to the train's transformer and traction system. The framework of a high-speed train pantograph coupling system is shown in Figure 1. It includes the pantograph-catenary coupling, wheel-rail contact, and fluid-structure coupling, which are characterised by strong nonlinear relationships. The system has numerous vibration sources, such as the unevenness of the catenary, posture changes of the car body induced from aerodynamic forces, track irregularities, and aerodynamic forces, resulting in complex vibrations and compound action. As an articulated mechanical component, the pantograph only relies on its own structure to maintain contact with the contact wire, and its dynamic behaviour is easily affected by excitation. The dynamic coupling performance of the pantograph determines whether it can stably and reliably take the electricity from the catenary.

Numerous theoretical analyses, simulations, and experimental studies of pantographs have been conducted, achieving significant progress. For example, Dai et al. [1,2] and Li et al. [3] studied the effect of strip spacing on the aerodynamics and aerodynamic noise

CONTACT Yi Guo guoyi0536@163.com

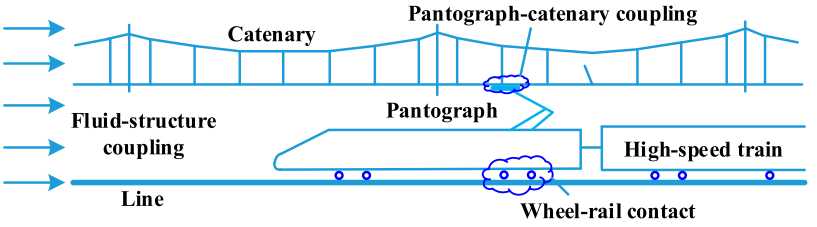

Figure 1. Framework of a high-speed train pantograph coupling system.

characteristics of high-speed train pantographs. Only the aerodynamics of high-speed train pantographs were considered. Dynamic analyses of pantograph – catenary systems were conducted under different operating conditions [4–12]; however, the influences of aerodynamic loads were not considered. Zhou et al. [13] investigated the dynamic characteristics of the pantograph, considering the influences of the pantograph's longitudinal impact and lateral swing, elastic vibration, airflow disturbance, and contact morphology. But the airflow disturbance was obtained from an aerodynamics calculation. Carnevale et al. [14] estimated the influence of aerodynamic forces on the contact force between the pantograph and catenary by calculating the fluid lift. The effect of vehicle body vibration on the pantograph – catenary system was analyzed according to the vibration responses of the vehicle roof. These responses were used as the excitation input into the pantograph – catenary model. Li et al. [15] found that the mean lift of the pantograph was 13.48% higher and the maximum exit lift was 34.3% higher when passing through a tunnel than when travelling in the open air. Zhang and Zeng [16] determined that the difference in the contact force between the pantograph and catenary was about 10%, regardless of whether car body vibration was considered. Therefore, the influence of previously ignored factors is significant and intensifies the interactions among different excitations, presenting a new challenge to traditional mechanics analysis methods. The coupling effect between the pantograph and the surrounding air is especially pronounced when the train is operating at high speeds. Thus, unidirectional coupling between aerodynamics and structural dynamics does not reflect this interaction, making it difficult to reveal the effect of wind-induced vibration.

Pombo and Ambrósio [17] adopted a combination of multi-body dynamics and finite element analysis to determine the coupling effect between multi-rigid pantographs and a flexible catenary at 300 km/h. The authors used time-varying wind loads as external loads and considered the track disturbance. Nakade et al. [18] studied the lateral vibration of a high-speed train passing through a tunnel via loose coupling between the train and its surrounding air. Li et al. [19] analyzed the coupling between aerodynamics and multi-body dynamics for three car bodies under crosswinds. The multi-body dynamic calculation was not performed until the aerodynamic calculation had converged. The dynamic solution programme was embedded into the fluid calculation to avoid an information transmission lag. The spring approximation method and grid remeshing were adopted to update the grid during mesh reconstruction. However, the pantograph rods had relatively large rotations, and large forward motions coexisted with small attitude changes. A grid motion method with stronger deformability is urgently needed.

No studies have investigated the influence of car body vibration on the coupling effect between the pantograph and tunnel using tight coupling between aerodynamics and

multi-body dynamics. In our proposed method, the data are updated multiple times in a time step until both physical fields converge or the predetermined number of iteration times is reached. When the second-order time accuracy is used for both the fluid and structure, the tight coupling ensures that the overall time accuracy of the fluid-structure coupling method reaches the second order, which is one order higher than that of the traditional loose coupling method.

In summary, as the train speed has increased, the service conditions of the pantograph have deteriorated, and existing research has not provided sufficient insights. We use advanced computing algorithms and methods to consider the unevenness of the catenary, operating speed, vibration from the car body roof, tunnel effect and fluid-structure coupling, and from multiple perspectives to describe and quantify the impact of changes in the car body's posture and track irregularities on the essential service characteristics and responses of the pantograph. The effects of the car body vibration on the pantograph and the tunnel coupling effect are investigated in-depth.

2. Model establishment

The pantograph consists of contact strips, contact strip supports and bracket, an upper arm, a lower arm, an upper pull rod, a lower pull rod, and a base frame; these are rigid bodies (Figure 1). The contact strips are attached to the supports, and the supports are connected to the bracket with two springs. The base frame is attached to the ground, and a spring for lifting the pantograph is connected to the base frame, which is connected to the lower arm. The other joints are hinged.

2.1. Multi-body dynamics model

The multi-body dynamics model of the pantograph is shown in Figure 2. The vertical dynamics equation for each rod of the pantograph is.

$$m\ddot{u} + c\dot{u} + ku = F_n + F_A + F_{link} \tag{1}$$

where m is the rod mass, c is the rod damper, k is the rod stiffness, u is the vertical displacement of the rod, and F_n is the contact force between the pantograph and catenary for the

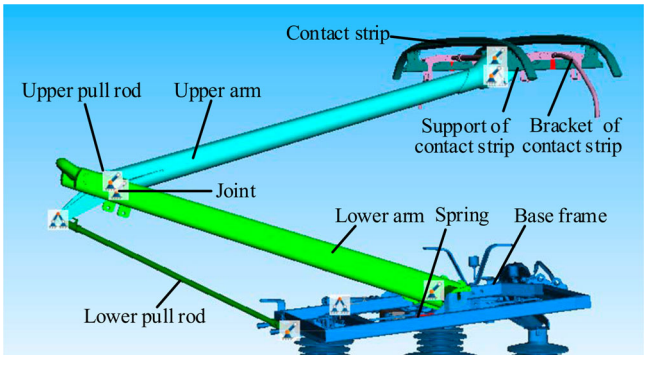

Figure 2. The multi-body dynamics model of the pantograph.

contact strip. F_n is 0 for the other rods. F_A is the aerodynamic force, and F_{link} is the total action force from other rods.

The contact force between the pantograph and catenary is defined as.

$$F_n = \begin{cases} k(x)r^{n(x)} + c(x)\dot{r}step(r-d) & r > 0 \\ 0 & r \le 0 \end{cases} \tag{2}$$

where x is the longitudinal displacement of the contact strip, $x = vt$, v is the operating speed of the train, and t is the operating time. The distance between the contact strip and catenary is $r = u_s - w_0$; u_s is the vertical displacement of the contact strip, w_0 is the unevenness of the catenary, $w_0(t) = 0.0055|\sin(2\pi vt/9.5)|$; $d = 0.0005m$; $n(x) = 1$; damper $c(x) = k(x)/100$; stiffness $k(x) = 7000 - (7000 - 5200)|\sin(\pi vt/9.5)|N/m$.

2.2. Aerodynamic model

The aerodynamic model considers the influences of the pressure wave caused by the head car and tail car entering and exiting the tunnel and of the car body on the flow field of the pantograph. Models of the head car, tail car, and middle car are established. The total operating distance is 800 m, the tunnel length is 480 m, and the cross-sectional area of the tunnel is 70 m^2. The numerical aerodynamic model is shown in Figure 3.

The Navier – Stokes equation can be used to describe the flow field of the high-speed train. If the mass force is neglected, the conservative Navier – Stokes equation can be written in the following vector form in the Cartesian coordinate system.

$$\frac{\partial \mathbf{U}}{\partial t} + \frac{\partial(\mathbf{E} - \mathbf{E}_v)}{\partial x} + \frac{\partial(\mathbf{F} - \mathbf{F}_v)}{\partial y} + \frac{\partial(\mathbf{G} - \mathbf{G}_v)}{\partial z} = 0, \tag{3}$$

where **U**, **E**, **F**, and **G** are the conserved variables and convective fluxes in the x, y, and z directions, respectively; they are expressed as follows

$$\mathbf{U} = \begin{pmatrix} \rho \\ \rho u \\ \rho v \\ \rho w \\ \rho e \end{pmatrix}, \mathbf{E} = \begin{pmatrix} \rho u \\ \rho u^2 + p \\ \rho uv \\ \rho uw \\ (\rho e + p)w \end{pmatrix}, \mathbf{F} = \begin{pmatrix} \rho v \\ \rho vu \\ \rho v^2 + p \\ \rho vw \\ (\rho e + p)v \end{pmatrix}, \mathbf{G} = \begin{pmatrix} \rho w \\ \rho uw \\ \rho vw \\ \rho w^2 + p \\ (\rho e + p)w \end{pmatrix}, \tag{4}$$

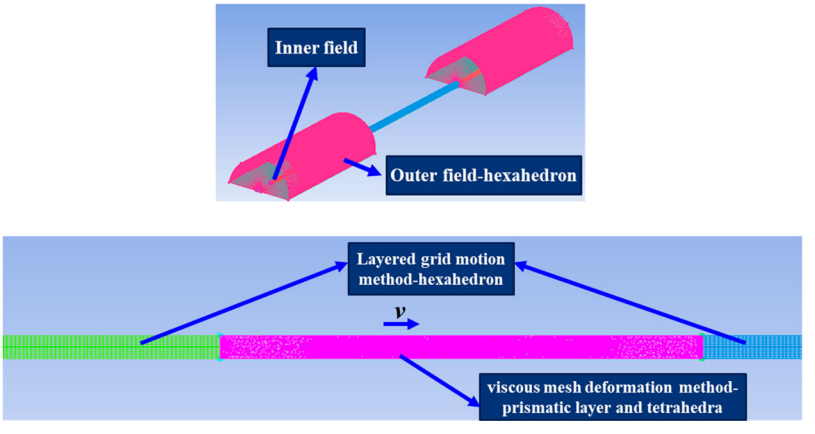

Figure 3. Numerical aerodynamic model.

where $\mathbf{E}_v$, $\mathbf{F}_v$, and $\mathbf{G}_v$ are the viscous fluxes in the x, y, and z directions, respectively; they are expressed as follows

$$\mathbf{E}_v = \begin{pmatrix} 0 \\ \tau_{xx} \\ \tau_{xy} \\ \tau_{xz} \\ u\tau_{xx} + v\tau_{xy} + w\tau_{xz} - q_x \end{pmatrix}, \mathbf{F}_v = \begin{pmatrix} 0 \\ \tau_{xy} \\ \tau_{yy} \\ \tau_{yz} \\ u\tau_{yx} + v\tau_{yy} + w\tau_{yz} - q_y \end{pmatrix},$$
$$\mathbf{G}_v = \begin{pmatrix} 0 \\ \tau_{xz} \\ \tau_{zy} \\ \tau_{zz} \\ u\tau_{zx} + v\tau_{zy} + w\tau_{zz} - q_z \end{pmatrix}. \tag{5}$$

The stress terms are expressed as

$$\begin{aligned} \tau_{xx} &= 2\mu u_x - \frac{2}{3}\mu(u_x + v_y + w_z);\ \tau_{xy} = \tau_{yx} = \mu(u_y + v_x); \\ \tau_{yy} &= 2\mu v_y - \frac{2}{3}\mu(u_x + v_y + w_z);\ \tau_{yz} = \tau_{zy} = \mu(v_z + w_y); \\ \tau_{zz} &= 2\mu w_z - \frac{2}{3}\mu(u_x + v_y + w_z);\ \tau_{xz} = \tau_{zx} = \mu(u_z + w_x). \end{aligned} \tag{6}$$

The heat conduction items are expressed as

$$q_x = -k\frac{\partial T}{\partial x},\ q_y = -k\frac{\partial T}{\partial y},\ q_z = -k\frac{\partial T}{\partial z}. \tag{7}$$

In Equations (3)–(7), u, v, and w are the directional components of the air velocity; p, T, k, and e are the pressure, temperature, heat conduction coefficient, and internal energy of air, respectively; μ is the viscosity coefficient.

The total energy e per unit mass of air is.

$$e = \frac{p}{(\gamma - 1)\rho} + \frac{u^2 + v^2 + w^2}{2} \tag{8}$$

where γ is the specific heat ratio.

It is necessary to use the gas state equation to close the Navier – Stokes equation.

$$p = \rho RT \tag{9}$$

3. Coupling between aerodynamics and multi-body dynamics

3.1. Proposed coupling method

The crucial aspects of the proposed method are the grid motion method and the data exchange. The grid motion method should match the grid type. The flow field of a pantograph on a high-speed train is divided into an inner field and an outer field, and a hybrid meshing method is adopted, as shown in Figure 3. The prismatic boundary layers around

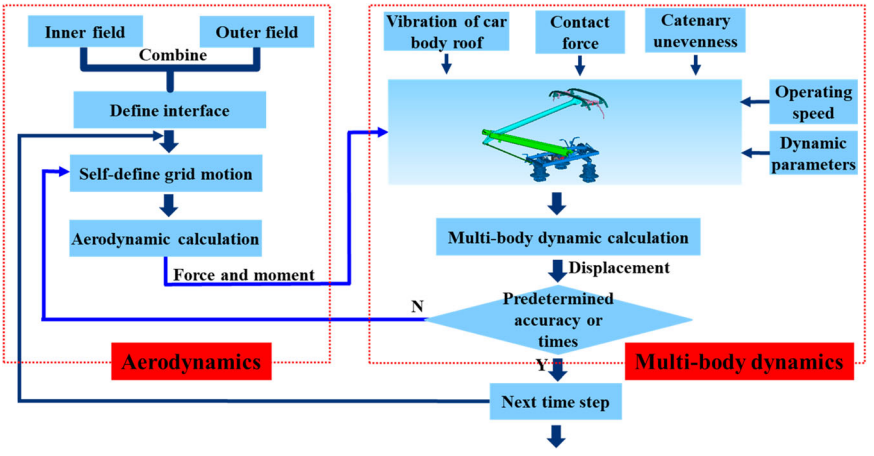

Figure 4. Flowchart of proposed coupling method.

the pantograph are used to describe the motion of the boundary and consider the viscous force at the surface. Due to the complex shape of the pantograph, a tetrahedral grid is used outside of the boundary layers because it is convenient for meshing. A hexahedral grid is used in the outer field since it is regular and easily adjusted. Data are exchanged through interfaces between the tetrahedral and hexahedral grids and the inner and outer fields. Layered grid motion is applied to the front and back of the inner field. It does not reduce the quality of the grid because the grid locations are updated. Viscous mesh deformation is applied to the flow field around the pantograph and the car body in the middle of the inner field by user self-defining. A two-step interpolation algorithm is used to ensure the calculation accuracy when the control points are selected. The control points are selected initially to prevent their update and to go through all of nodes on the rod roofs during computation to ensure high efficiency. The coordinates of the nodes surrounding the flow field are updated when the points are displaced. This strategy is suitable for the parallel processing of large-scale mesh deformation. The combination of the two methods ensures that the forward motion and posture changes of the pantograph are captured, and grid updating is performed accurately. A data file is used to exchange data between the aerodynamic and multi-body dynamic models because of its straightforward and fast implementation. The flowchart of the proposed coupling method is shown in Figure 4.

3.2. Verification of proposed coupling method

The contact forces between the pantograph and catenary were tested using an experiment at different train speeds. The fitted results of the maximum, minimum, and mean values at 100 m/s are listed in Table 1. The contact forces between the pantograph and catenary obtained from the coupled model are shown in Figure 5. The cases of bidirectional coupling, wind loads as known loads, no wind loads are conducted.

The following is observed in Figure 5 and Table 1.

(1) The trends of the contact force between the pantograph and catenary are similar but the values of the aerodynamic load differ for the three cases.

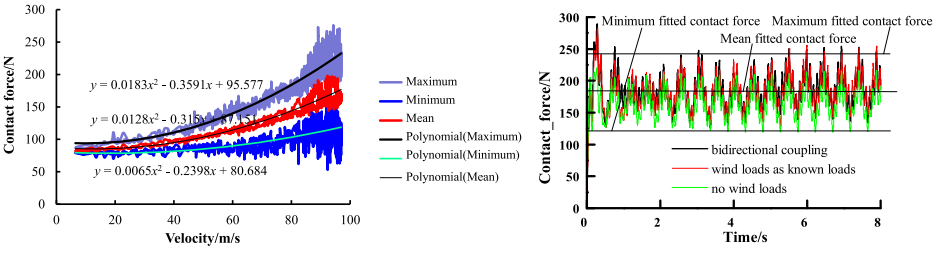

Figure 5. Fitted and simulated results of the contact forces between the pantograph and catenary at a train speed of 360 km/h in the open air.

Table 1. Statistical results of the simulated and fitted contact force between pantograph and catenary at 360 km/h in the open air.

	Maximum (N)	Minimum (N)	Mean (N)	Standard deviation (N)	Mean error	Minimum error
Bidirectional coupling	254.26	126.48	183.56	25.55	−0.05%	3.92%
Wind loads as known loads	255.98	129.58	182.59	25.03	−0.58%	6.47%
No wind loads	216.16	119.44	162.42	21.66	11.56%	−11.56%
Fitted results	242.67	121.70	183.65	-	-	-

(2) The contact forces between the pantograph and catenary are much smaller when the aerodynamic loads are not considered, indicating that the aerodynamic loads imposing the pantograph significantly impact the current collection when the train operates at high speed.
(3) The standard deviation of the contact force is larger in bidirectional coupling than when the aerodynamic loads are the known loads in the open-air case. This finding indicates that the contact force fluctuates substantially, and the performance of current collection is low.
(4) The bidirectional coupling results are closer to the test results regardless of the maximum, minimum, or mean values.

According to the verification standard of dynamic simulation between the pantograph and catenary (EN50318), the mean contact force $F_m \leq 0.00094 \times 360^2 + 70 = 195.712N$, and the standard deviation of the contact force $\sigma_{\max} = 58.7136N$. Thus, all the simulation and experimental results meet the requirements.

4. Results and discussion

To study the influences of car body vibration on coupling effect between pantograph and tunnel at different speeds, we consider four cases: with/without car body vibration at speeds of 360 and 420 km/h while travelling through a tunnel. The coupled aerodynamic and multi-body dynamic model is used for all cases. The case without car body vibration at 360 km/h is used as the benchmark in this section. Due to the large mass of the train, the effect of the pantograph on the body vibration can be ignored, but the vibration of the car body roof has a significant impact on the pantograph. Therefore, the vibration of the car body roof on the base of the pantograph is regarded as a known condition. The results are shown in Figure 6 (a)-(d) and Tables 2–5.

4.1. Time-domain characteristics

4.1.1. Aerodynamic lift

The panhead is composed of contact strips, supports, and a bracket. The comparison of the aerodynamic lift of the panhead with or without car body vibration as the train travels through the tunnel at 360 and 420 km/h is shown in Figure 6(a). Negative values indicate

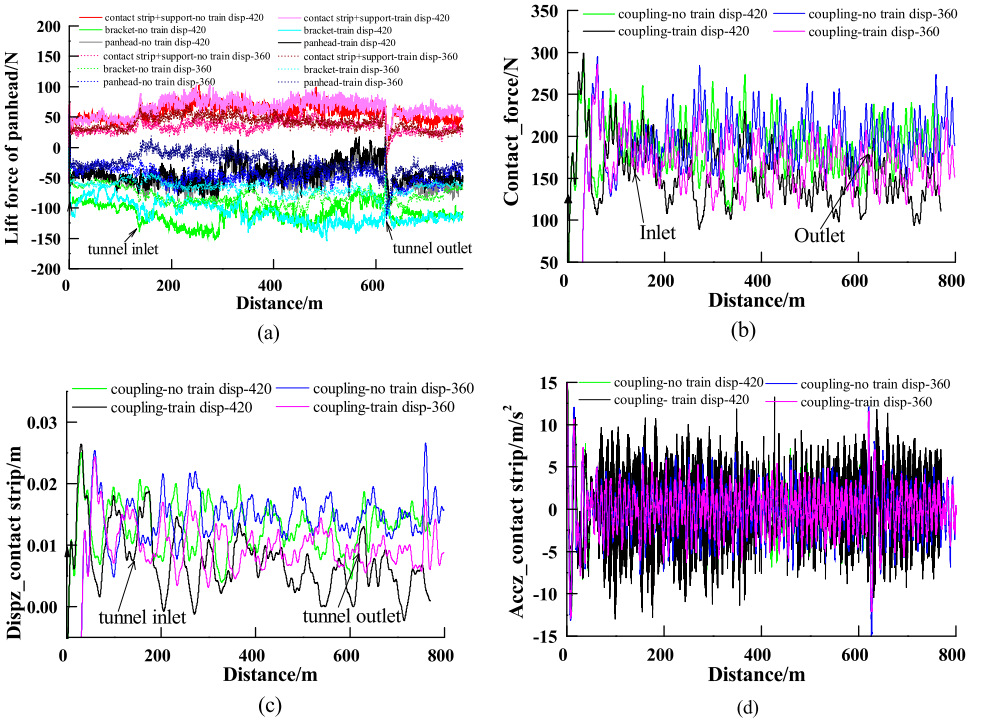

Figure 6. Calculation results for different cases of the train travelling through a tunnel with or without car body vibration. (a) Aerodynamic lift of the panhead; (b) Contact force between the pantograph and catenary; (c) Vertical displacement of the contact strip; (d) Vertical acceleration of the contact strip.

Table 2. Statistical results of the aerodynamic lift of the panhead with or without car body vibration as the train passes through the tunnel.

	Maximum (N)	Minimum (N)	Mean (N)	Standard deviation (N)	Standard deviation difference	Mean difference
Contact strip +support-no train disp-360	67.71	−25.55	33.76	9.69	-	-
Bracket-no train disp-360	−43.63	−111.31	−81.01	12.60	-	-
Panhead-no train disp-360	2.83	−110.03	−47.25	13.16	-	-
Contact strip +support-train disp-360	71.92	−37.70	39.96	11.54	19.09%	18.36%
Bracket-train disp-360	−41.11	−114.39	−66.31	9.82	−22.06%	−18.15%
Panhead-train disp-360	19.01	−124.97	−26.35	15.18	15.35%	−44.23%
Contact strip +support-no train disp-420	102.57	10.03	58.28	12.98	33.95%	72.63%
Bracket-no train disp-420	−50.08	−152.78	−109.50	16.78	33.17%	35.17%
Panhead-no train disp-420	18.26	−96.32	−51.22	17.33	31.69%	8.40%
Contact strip +support-train disp-420	103.65	10.93	65.18	13.74	41.80%	93.07%
Bracket-train disp-420	−60.94	−153.72	−107.63	17.50	38.89%	32.86%
Panhead-train disp-420	17.70	−96.20	−44.32	17.22	30.85%	−6.20%

Table 3. Statistical results of the contact force between pantograph and catenary with or without car body vibration as the train passes through the tunnel.

	Maximum (N)	Minimum (N)	Mean (N)	Standard deviation (N)	Standard deviation difference	Minimum difference
Coupling-no train disp-360	293.89	127.55	196.55	28.08	-	-
Coupling-train disp-360	284.86	107.22	165.18	27.67	−1.46%	−15.94%
Coupling-no train disp-420	292.64	110.55	186.40	29.77	6.02%	−13.33%
Coupling-train disp-420	299.08	88.99	153.09	34.28	22.08%	−30.23%

Table 4. Statistical results of the vertical displacement of the contact strip with or without car body vibration as the train passes through the tunnel.

	Maximum (m)	Minimum (m)	Mean (m)	Standard deviation (m)	Standard deviation difference	Mean difference
Coupling-no train disp-360	0.02650	0.00469	0.01468	0.00310	-	-
Coupling-train disp-360	0.02421	0.00301	0.00936	0.00336	−8.39%	−36.24%
Coupling-no train disp-420	0.02498	0.00398	0.01293	0.00387	24.84%	−11.92%
Coupling-train disp-420	0.02645	−0.00226	0.00731	0.00509	64.19%	−50.20%

Table 5. Statistical results of the vertical acceleration of the contact strip with or without car body vibration as the train passes through the tunnel.

	Maximum (m/s^2)	Minimum (m/s^2)	Mean (m/s^2)	Standard deviation (m/s^2)	Standard deviation difference	Minimum difference
Coupling-tunnel-no train disp-360	12.11	−15.09	0.01	3.10	-	-
Coupling-tunnel-train disp-360	11.61	−12.11	0.01	2.62	−15.48%	−19.79%
Coupling-tunnel-no train disp-420	10.07	−8.35	0.02	2.94	−5.16%	−44.67%
Coupling-tunnel-train disp-420	13.31	−12.99	0.01	3.63	17.10%	−13.92%

uplift forces. Their statistical results are listed in Table 2. In which, the case of 'Contact strip +support-no train disp-360' is the aerodynamic lift acted on the contact strips and supports without car body vibration at 360 km/h, the case of 'Bracket-no train disp-360' is the aerodynamic lift acted on the bracket without car body vibration at 360 km/h, and the case of 'Panhead-no train disp-360' is the aerodynamic lift acted on the panhead without car body vibration at 360 km/h. The meanings of the others are and all that.

The following is observed in Figure 6 (a) as follows.

(1) The direction of the aerodynamic lift of the contact strip-support is opposite to that of the bracket, except at the tunnel exit, and the values are smaller than that of the bracket.
(2) At the same speed, the aerodynamic lift differences between the cases with and without car body vibration are larger inside the tunnel than outside the tunnel, indicating a significant tunnel effect.
(3) The aerodynamic lift values of the contact strip-support and bracket are larger at 420 km/h than at 360 km/h. However, their sum, i.e. the aerodynamic lift of the panhead, does not exhibit the same trend.

(4) The downward aerodynamic lift of the contact strip-support is larger and the total aerodynamic lift of the panhead is smaller with than without car body vibration. Downward lift also occurs when the car body vibration is considered and is a primary reason for the separation between the pantograph and catenary.
(5) Significant alternations occur between the uplifting force and downward force at the tunnel exits for all four cases.

The following findings are observed in Table 2.

(1) The minimum aerodynamic lift of the panhead is substantially lower at 360 km/h than at 420 km/h, and the differences in the standard deviation between at 360 km/h without car body vibration and at 420 km/h without and with car body vibration are 31.69% and 30.85%, respectively. The mean differences are 8.40% and −6.20%.
(2) The standard deviation of the total aerodynamic lift of the panhead is lower without car body vibration (13.16 N) than with vibration (15.18 N) at 360 km/h and is higher without vibration (17.33 N) than with vibration (17.22 N) at 420 km/h.

4.1.2. Contact force between pantograph and catenary

Figure 6(b) and Table 3 show the comparison of the contact force between the pantograph and catenary and the statistical results with or without car body vibration when the train passes through the tunnel at 360 and 420 km/h. The following is observed.

(1) The peaks and valleys of the contact force curves are the opposite at 420 and 360 km/h at some positions, such as at 60, 206, and 337 m.
(2) The maximum and minimum values of the contact force between the pantograph and catenary are mostly smaller at 420 km/h than at 360 km/h, whereas the standard deviation is larger. For example, the minimum value is 13.33% lower, and the standard deviation is 6.02% higher at 420 km/h than at 360 km/h without vibration. The standard deviation is 22.08% higher, and the minimum value is 30.23% lower at 420 km/h than at 360 km/h with vibration. When other excitations occur at higher speed, the separation between the pantograph and catenary and arcing are likely.
(3) At the same speed, the contact force between the pantograph and catenary is usually lower with than without car body vibration in figure 6.
(4) The car body vibration has a more significant influence on the contact force between the pantograph and catenary inside than outside the tunnel.

4.1.3. Vertical displacement of the contact strip

Figure 6(c) and Table 4 show the comparison of the contact strip vertical displacement and the statistical results, respectively, with or without car body vibration as the train travels through the tunnel at 360 and 420 km/h. The following is observed.

(1) The peaks and valleys of the vertical displacement of the contact strip are the opposite at 360 km/h and at 420 km/h at some positions, such as at 60, 100, 204, 234, and 328 m.
(2) The mean value of the vertical displacement of the contact strip is lower, and the standard deviation is higher at 420 km/h than at 360 km/h. For example, the mean value is 11.92% lower, and the standard deviation is 24.84% higher at 420 km/h than at 360

km/h without car body vibration. The mean value is 50.20% lower, and the standard deviation is 64.19% higher with car body vibration.

(3) At the same speed, the vertical displacement of the contact strip is lower with than without car body vibration in Figure 6(c). However, the standard deviation is higher. For example, it increases from 0.00310–0.00366 m at 360 km/h and from 0.00387–0.00509 m at 420 km/h.

(4) Negative displacement occurs at 420 km/h with car body vibration, indicating that the contact strip has moved below the equilibrium position, increasing the likelihood of separation from the catenary.

4.1.4. Vertical acceleration of the contact strip

Figure 6(d) and Table 5 show the comparison of the vertical acceleration of the contact strip and the statistical results, respectively, with or without car body vibration when the train passes through the tunnel at 360 and 420 km/h. The following is observed.

(1) The car body vibration has a much greater influence on the vertical acceleration of the contact strip at 420 km/h than at 360 km/h in Figure 6(d).

(2) The maximum, minimum, and standard deviation of the vertical acceleration of the contact strip are lower at 420 km/h than at 360 km/h without car body vibration. The values are higher at 420 km/h than at 360 km/h with car body vibration.

(3) The standard deviation of the vertical acceleration of the contact strip decreases from 3.10 m/s^2 with vibration to 2.62 m/s^2 without vibration at 360 km/h and increases from 2.94 m/s^2 with vibration to 3.63 m/s^2 without vibration at 420 km/h.

(4) The maximum and minimum values of the vertical acceleration of the contact strip are lower with than without car body vibration at 360 km/h and higher at 420 km/h.

4.2. Frequency-domain characteristics

The power spectral density (PSD) curves of the contact force between the pantograph and catenary, the vertical displacement, and the vertical acceleration of the contact strip are shown in Figure 7 with or without car body vibration when the train travels through the tunnel at 360 and 420 km/h. The following is observed.

(1) The basic frequency of the contact force between the pantograph and catenary is 2.11 Hz. At the frequency and multiples of the frequency (3, 5, 6, 10, 15, 20, 25, 30, and 35 times), PSDs of the contact force are larger. Higher frequencies occur. The line test data after filtering at 20 Hz are insufficient for high-speed pantographs.

(2) PSD of the contact force between the pantograph and catenary is smaller with than without car body vibration at the same speed.

(3) The main frequencies corresponding to larger PSDs for the contact force between the pantograph and catenary are the same with or without car body vibration at the same speed. Conversely, the main frequencies are different at different speeds.

(4) The basic frequency of the vertical displacement of the contact strip is 2.11 Hz, and PSDs are larger at the frequency and multiples of the frequency (2, 3, and 5 times). The largest PSDs occur around 1.75 Hz, which is not both the basic frequency and multiples of the basic frequency.

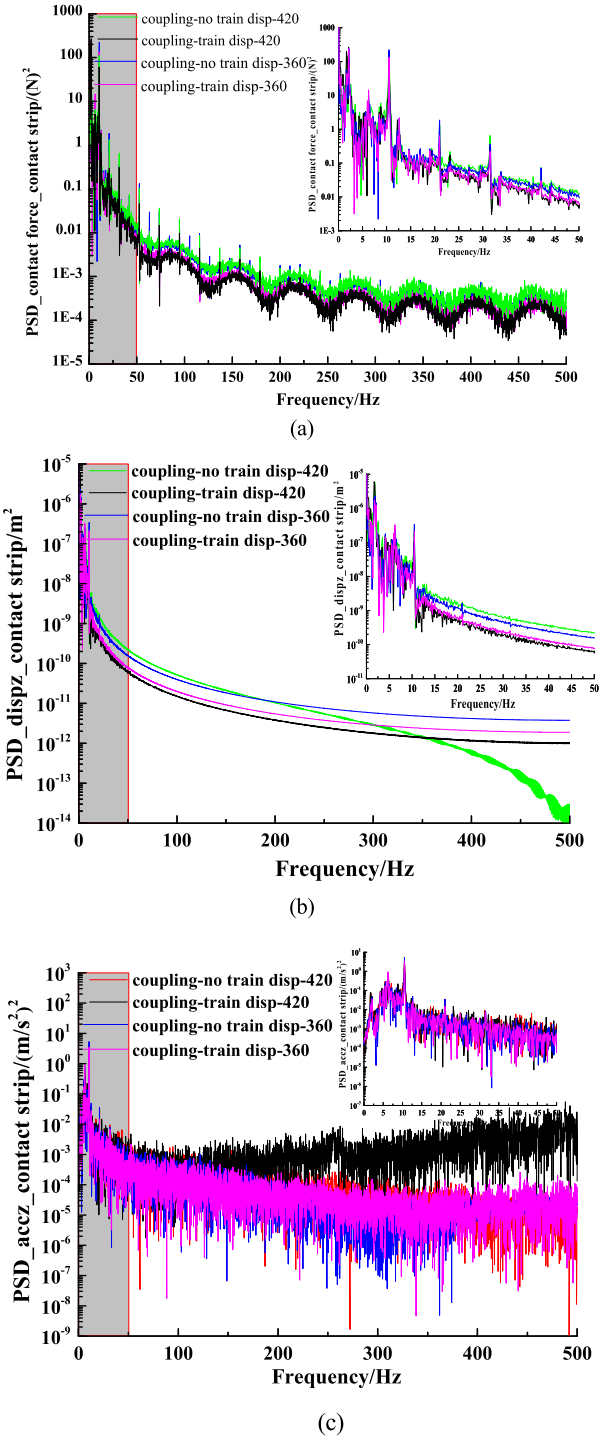

Figure 7. Power spectral density curves with or without car body vibration as the train passes through the tunnel. (a) Contact force between pantograph and catenary; (b) Vertical displacement of the contact strip; (c) Vertical acceleration of the contact strip.

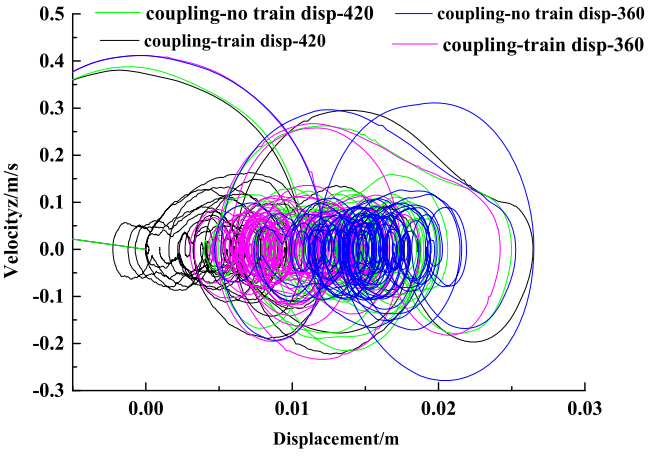

Figure 8. Phase diagram of the contact strip with or without car body vibration.

(5) PSDs of the vertical displacement of the contact strip are below 10 Hz with or without car body vibration at the same speed. Over 10 Hz, the amplitudes are smaller but fluctuate more with car body vibration than without car body vibration. However, the amplitudes decay sharply from 350 Hz at 420 km/h without car body vibration, and the amplitude fluctuations increase with an increase in frequency.
(6) The basic frequency of the vertical acceleration of the contact strip is 2.11 Hz, and PSDs are larger at the frequency and multiples of the frequency (3, 4, 5, 10, and 15 times). The largest PSDs occur around 10.50 Hz.
(7) PSDs of the vertical acceleration of the contact strip are larger with than without vibration at the same speed and show an increasing trend, especially at 420 km/h.

4.3. Phase diagram of the contact strip

Figure 8 shows the phase diagram of the contact strip with or without car body vibration as the train passes through the tunnel at 360 and 420 km/h. The following is observed.

(1) The attractors are observed at the left and right ends and show signs of entering a chaotic state at both speeds and with or without car body vibration.
(2) The phase diagram of the case with car body vibration is significantly more extended to the left than that without car body vibration.
(3) The phase diagram for a speed of 420 km/h is significantly more extended to the left than that for a speed of 360 km/h, and negative displacement occurs.
(4) The phase diagram of the case with car body vibration and a speed of 420 km/h exhibits irregular curves at many locations, and there are several discontinuous rings at the left end.

5. Conclusions

A new coupling method between aerodynamics and multi-body dynamics was presented to investigate the complex vibration and compound action of the pantograph of a high-speed

train. The catenary unevenness, car body posture changes, track irregularities, tunnel effect, and interactions between the air and the rods were considered, and the influences of the car body vibration on the service characteristics and responses of the pantograph were analyzed in-depth from multiple perspectives. The main conclusions were as follows.

(1) The downward aerodynamic lift of the contact strip-support was larger, and the total aerodynamic lift of the panhead was smaller with than without car body vibration. The panhead exhibited downward lift appearing, which was the primary reason for the separation between the pantograph and catenary when car body vibration was considered.
(2) The minimum value of the contact force between the pantograph and catenary was 13.33% lower, the standard deviation was 6.02% higher, the mean vertical displacement of the contact strip was 11.92% lower, and the standard deviation was 24.84% higher at 420 km/h than at 360 km/h without car body vibration.
(3) The minimum value of the contact force between the pantograph and catenary was 30.23% lower, the standard deviation was 22.08% higher, the mean vertical displacement of the contact strip was 50.20% lower, and the standard deviation was 64.19% higher at 420 km/h than at 360 km/h with car body vibration.
(4) However, PSDs of the vertical displacement of the contact strip decayed sharply from 350 Hz and were higher at higher frequencies at 420 km/h than at 360 km/h without car body vibration.

Disclosure statement

No potential conflict of interest was reported by the author(s).

Funding

This work was supported by the National Natural Science Foundation of China [grant no 52172336], the Strategic Priority Research Program of the Chinese Academy of Sciences (Class B) [grant no XDB22020101], and the Research Project of the Chinese Academy of Sciences [grant no XXH13506-204].

ORCID

Jun Mao http://orcid.org/0000-0003-3984-4115

References

[1] Dai ZY, Li T, Deng J, et al. Effect of the strip spacing on the aerodynamic performance of a high-speed double-strip pantograph. Veh Syst Dyn. 2021;60(10):3358–3374. doi:10.1080/00423114.
[2] Dai ZY, Li T, Zhang WH, et al. Numerical study on aerodynamic performance of high-speed pantograph with double strips. Fluid Dyn Mater Process. 2020;16(1):31–40.
[3] Li T, Qin D, Zhang WH, et al. Study on the aerodynamic noise characteristics of high-speed pantographs with different strip spacings. J Wind Eng Ind Aerodyn. 2020;202:1–19.
[4] Simarro M, Postigo S, Prado-Novoa M, et al. Analysis of contact forces between the pantograph and the overhead conductor rail using a validated finite element model. Eng Struct. 2020;225:1–15.

[5] Song Y, Rønnquist A, Nåvik P. Assessment of the high-frequency response in the railway pantograph-catenary interaction based on numerical simulation. IEEE Trans Veh Technol. 2020;69(10):1–10.
[6] Yao YM, Zhou N, Mei GM. Dynamic analysis of pantograph-catenary system considering ice coating. Shock Vib. 2020;1:1–15.
[7] Song Y, Liu Z, Rønnquist A, et al. Contact wire irregularity stochastics and effect on high-speed railway pantograph-catenary interactions. IEEE Trans Instrum Meas. 2020;69:8196–8206.
[8] Zhai WM, Cai CB. Effect of locomotive vibrations on pantograph-catenary system dynamics. Veh Syst Dyn. 1998;29(S1):47–58.
[9] Carnicero A, Jimenez-Octavio JR, Sanchez-Rebollo C, et al. Influence of track irregularities in the catenary-pantograph dynamic interaction. J Comput Nonlinear Dyn. 2012;7:1–20.
[10] Abdullah MA, Ibrahim A, Michitsuji Y, et al. Active control of high-speed railway vehicle pantograph considering vertical body vibration. Int J Mech Eng Technol. 2013;4(6):263–274.
[11] Yao YM, Zou D, Zhou N, et al. A study on the mechanism of vehicle body vibration affecting the dynamic interaction in the pantograph–catenary system. Veh Syst Dyn. 2020;3:1–20.
[12] Song Y, Wang ZW, Liu ZG, et al. A spatial coupling model to study dynamic performance of pantograph-catenary with vehicle-track excitation. Mech Syst Signal Process. 2021;151:1–26.
[13] Zhou N, Zou H, Li R, et al. Dynamic behavior of different pantograph models in simulation of pantograph and catenary interaction, 2016 Proceedings of the 35th Chinese Control Conference, Chengdu, China, (2016) 10242-10247.
[14] Carnevale M, Facchinetti A, Maggiori L, et al. Computational fluid dynamics as a means of assessing the influence of aerodynamic forces on the mean contact force acting on a pantograph. J Rail Rapid Transit. 2016;230:1698–1713.
[15] Li RP, Zhang WH, Ning Z, et al. Influence of a high-speed train passing through a tunnel on pantograph aerodynamics and pantograph–catenary interaction. J Rail Rapid Transit. 2017;231:198–210.
[16] Zhang WH, Zeng J. A review of vehicle system dynamics in the development of high-speed trains in China. Int J Dyn Control. 2013;1:81–97.
[17] Pombo J, Ambrósio J. Environmental and track perturbations on multiple pantograph interaction with catenaries in high-speed trains. Comput Struct. 2013;124:88–101.
[18] Nakade K, Masahiro S, Hiroshi F. Interaction between vehicle vibration and aerodynamic force on high-speed train running in tunnel. Veh Syst Dyn. 2004;41:717–723.
[19] Li T, Zhang JY, Zhang WH. An improved algorithm for fluid-structure interaction of high-speed trains under crosswind. J Mod Transp. 2011;19:75–81.